Liquid-Core Microstructured Polymer Optical Fiber as Fiber-Enhanced Raman Spectroscopy Probe for Glucose Sensing

Mikel Azkune, Timea Frosch, Eneko Arrospide, Gotzon Aldabaldetreku, Iñaki Bikandi, Joseba Zubia, Jürgen Popp, and Torsten Frosch

***Abstract*—This work reports the development and application of two liquid-core microstructured polymer optical fibers (LC-mPOF) with different microstructure sizes. They are used in a fiber-enhanced Raman spectroscopy sensing platform, with the aim of detecting glucose in aqueous solutions in the clinically relevant range for sodium–glucose cotransporter 2 inhibitor therapy. The sensing platform is tested for low-concentration glucose solutions using each LC-mPOF. Results confirm that a significant enhancement of the Raman signal is achieved in comparison to conventional Raman spectroscopy. Additional measurements are carried out to obtain the valid measurement range, the resolution, and the limit of detection, showing that the LC-mPOF with 66-μm-diameter central hollow core has the highest potential for future clinical applications. Finally, preliminary tests successfully demonstrate glucose identification in urine.**

***Index Terms*—Fiber enhanced Raman spectroscopy, glucose sensing, hollow-core microstructured polymer optical fibers.**

I. Introduction

ACCORDING to the World Health Organization, approximately 150 million people are suffering from diabetes mellitus worldwide. It is estimated that this number may well double by 2025. Much of this increase will take place in developing countries due to population growth, aging, obesity, and unhealthy lifestyle [1]. Therefore, it is necessary to find the right antidiabetic therapy so as to avoid unwanted adverse effects and/or hypo- and hyperglycemic conditions. For such a purpose, non-invasive therapeutic drug monitoring would be beneficial, especially during the sodium-glucose co-transporter 2 (SGLT2) inhibitor therapy. More specifically, these oral antidiabetic drugs decrease plasma glucose levels by inhibiting the SGLT2 enzyme, which is responsible for the reabsorption of filtered glucose in the kidneys, so that there is an increase in the urinary glucose excretion [2]. There are additional benefits to using SGLT2 inhibitors for diabetic patients, since they lower the blood pressure and improve the weight loss [3]. However, urinary and genital infections are more common due to the higher levels of glucose in the urinary tract [2]. In fact, the Food and Drug Administration (FDA) has issued a public health advisory for prescribers and users of SGLT2 inhibitor therapy about rare but severe infections of the genitals [4]. Kim *et al*. recently proposed that the combined monitoring of urinary glucose levels and blood glucose indices might be a better indicator of glycemic control in patients under SGLT2 inhibitor treatment [5]. Thus, it would be of great interest to have at disposal a quick, non-invasive, easy-to-use and low-cost method to monitor patients' urinary glucose levels.

Raman spectroscopy is an arising vibrational spectroscopic method that fulfills previous requirements. Some early studies used Raman spectroscopy for glucose quantification by means of different enhancement techniques [6]–[8]. A very promising enhancement technique is based on optical fibers [9], [10], more especially, using hollow-core microstructured optical fibers [11]–[13]. These fibers provide longer interaction lengths between the sample and light, and they guide the scattered light inside the central core, leading to a considerable enhancement of the Raman signal of the target sample. This technique is called Fiber Enhanced Raman Spectroscopy (FERS) [14]. In fact, this technology has widely been used in silica fibers [12], [15]–[17], but it is not yet elucidated in polymer optical fibers (POF).

Thus, this work introduces a new approach for sensitive glucose quantification, relying on a specifically designed and fabricated microstructured polymer optical fiber (mPOF) made by

Manuscript received November 26, 2018; revised March 15, 2019; accepted March 28, 2019. Date of publication April 1, 2019; date of current version May 24, 2019. This work was supported in part by European Regional Development Fund, in part by the Ministerio de Economía y Competitividad under Project TEC2015-638263-C03-1-R, in part by Gobierno Vasco/Eusko Jaurlaritza under Projects IT933-16 and ELKARTEK (KK-2016/0030, KK-2017/00033, KK-2017/00089, and KK-2016/0059), and in part by the Free State of Thuringia, Germany (2015 FE 9012). The work of M. Azkune was supported in part by a research fellowship from the University of the Basque Country, Vicerrectorado de Euskera y Formación Continua. *(Corresponding author: Mikel Azkune.)*

M. Azkune, G. Aldabaldetreku, I. Bikandi, and J. Zubia are with the Department of Communications Engineering, Faculty of Engineering, University of the Basque Country, Bilbao 48013, Spain (e-mail: mikel.azkune@ehu.eus; gotzon.aldabaldetreku@ehu.eus; inaki.bikandi@ehu.es; joseba.zubia@ehu.es).

T. Frosch is with the Leibniz Institute of Photonic Technology, Jena 07745, Germany (e-mail: timea.frosch@leibniz-ipht.de).

E. Arrospide is with the Department of Applied Mathematics, Faculty of Engineering, University of the Basque Country, Bilbao 48013, Spain (e-mail: eneko.arrospide@ehu.eus).

J. Popp and T. Frosch are with the Leibniz Institute of Photonic Technology, Jena 07745, Germany, and also with Abbe Centre of Photonics and Institute of Physical Chemistry, Friedrich Schiller University, Jena 07745, Germany (e-mail: juergen.popp@uni-jena.de; torsten.frosch@uni-jena.de).

Color versions of one or more of the figures in this paper are available online at http://ieeexplore.ieee.org.

Digital Object Identifier 10.1109/JLT.2019.2908447

poly(methyl methacrylate) (PMMA). The cladding region of the mPOF consists of a periodic holey-structure surrounding the liquid-filled core. This configuration enables the transmission of light through the liquid-core mPOF (LC-mPOF). Since the effective refractive index of the cladding decreases below the aqueous-like refractive index of the selectively-filled core, light transmission is confined to the core due to the modified total internal reflection (MTIR) mechanism. This mechanism suits better the purposes of this sensing platform in comparison to the band-gap guiding mechanism because the latter provides narrower transmission windows and these windows also shift when the probe is filled with an aqueous solution, so that light transmission by band-gap guiding mechanism is more restrictive for FERS measurements [18]. Therefore, ad-hoc designed LC-mPOF can overcome the poor efficiency of the Raman scattering in the analysis of biological solutions in comparison to conventional Raman measurements.

The main advantages of mPOFs, in contrast to their silica counterparts, are their lower production cost, their flexibility and their bio-compatibility. Therefore, mPOFs exhibit great potential for clinical applications. Additionally, thanks to their lower melting temperature, the inner wall surface can be functionalized in order to increase sensitivity [19]. Nevertheless, polymer fibers based on PMMA suffer from strong Raman background signal, even though this background signal can be removed by means of a correct signal processing, since the Raman peaks of PMMA have already been studied in the literature [20], [21]. In any case, potassium ferricyanide ($K_3[Fe(CN)_6]$) has been added to the glucose solutions in order to make easier the measurement of the Signal-to-Noise Ratio (SNR), because the potassium ferricyanide shows a unique Raman peak outside the spectral region of the Raman peaks of PMMA.

This manuscript reports an LC-mPOF based FERS sensing platform for glucose sensing. First, it describes in detail the fabrication steps of the designed mPOFs, from the initial preform to the final LC-mPOF. Afterwards, experimental measurements are carried out in Section II to prove the feasibility of the sensing platform for use in low-concentration glucose solutions, showing its potential for monitoring in SGLT2 inhibitor therapy. Then, Section III discusses the results, showing the potential of the LC-mPOF platform for SGLT2 inhibitor therapy monitoring. Finally, the main conclusions drawn from the work are summarized in Section IV.

II. Experimental

A. Materials

All the solutions used in this work were prepared using deionized water as a solvent. The α-D-glucose and the potassium ferricyanide ($K_3[Fe(CN)_6]$) were purchasedt from Sigma-Aldrich (St. Louis, Mo, USA). The urine was provided by a donor. The end-faces of the fibers were sealed using an optical adhesive NOA 65 purchased from Norland Products (Cranbury, NJ, USA). The base material for the preforms was PMMA of optical quality (Plexiglass). They were delivered in 60-mm-diameter rods by Evonik (Essen, Germany).

Fig. 1. Digital camera photograph of the drilled preform with a diameter of 60 mm.

B. mPOF Fabrication

LC-mPOF probes must fulfill some special conditions for FERS measurements that, in spite of being conceptually simple, are not easily met and, consequently, a lot of experience in mPOF fabrication is required [22]. On the one hand, the diameter of the central hole has to be big enough so as to be filled by the solution containing the target sample. On the other hand, the diameters of the holes of the cladding have to be remarkably smaller than the central hole in order to enable the use of the selective filling technique, which is explained below. It is important to bear in mind that the air fraction of the cladding region has to be high enough to decrease the effective refractive index of the cladding below the refractive index of the liquid-filled core (the latter is almost similar to the refractive index of the solution containing the target sample). This configuration ensures that light will be confined into the core by means of the MTIR guiding mechanism.

The chosen geometry that fulfills these requirements consists in a six-ring cladding and a central hollow-core. Two different core sizes have been fabricated in order to find out the design of better performance in the FERS sensing platform: both designs maintain the same geometry and they have been obtained by modifying some parameters in the mPOF drawing stage.

1) Preform Fabrication: The chosen structure was drilled in a solid PMMA rod with a diameter of 60 mm and a length of 120 mm. The solid PMMA rod was drilled using a numerical control machine and internally refrigerated carbide drill bits. The obtained preform is shown in Fig. 1. Afterwards, the preform was cleaned and stored in low-humidity (20%) and high-temperature (80 °C) conditions for several days with the aim of removing all humidity, residual stress, and monomer remnants so as to maintain the quality of the mPOF.

2) Fiber Drawing: Afterwards, the drilled preform was drawn employing a two-step process [22]. In the first one, the preform was stretched to a 3-mm-diameter intermediate cane (Fig. 2a) and, then, the cane was sleeved with a PMMA tube, obtaining the secondary preform.

In the second step, the secondary preform was drawn to the final mPOF (Fig. 2b). The geometry of the final mPOF can be adjusted by tuning the drawing speed or the air pressure delivered to the cladding and core holes, either positive or negative. On the

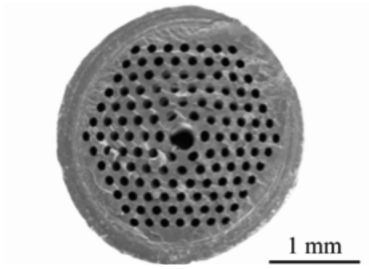

a) Image of the cane (intermediate fabrication step).

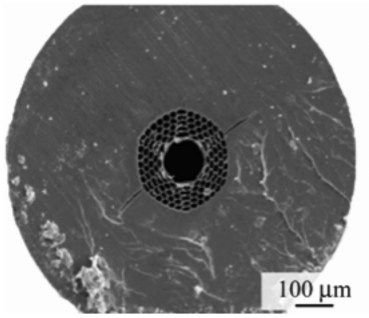

b) Image of the final fiber (final fabrication step).

Fig. 2. SEM images of the mPOF end-face at each fabrication step.

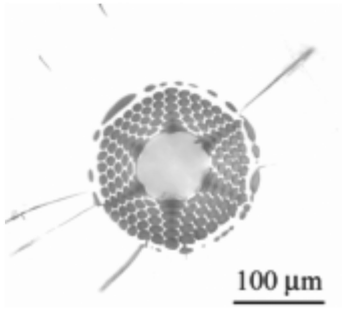

a) 66 ϕ LC-mPOF.

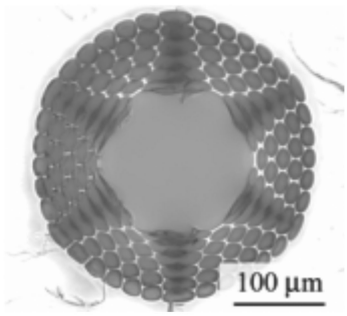

b) 100 ϕ LC-mPOF.

Fig. 3. Microscope photographs of the mPOF microstructure for both fiber sizes.

one hand, the faster the drawing speed, the smaller the obtained fiber diameter. On the other hand, if the air pressure is altered, the diameters of the holes tend to expand or collapse.

This way, a small-size core mPOF was obtained with a faster drawing speed but lower pressure in the central core. In contrast, for a big-size core mPOF, the drawing speed was slower but the pressure in the central core higher. As a result, the same microstructure was reproduced in two different sizes as can be seen in Figs. 3a and b. In order to demonstrate that both fiber sizes have the same geometry but different on scale, the dimensionless core-cladding ratio has been used. Thus, the small-size fiber has a 66-μm-diameter central hollow-core and an external diameter of 660 μm with a core-cladding ratio of 0.42, whereas the big-size fiber has a 100 μm wide central hollow-core and an external diameter of 1 mm with a core-cladding ratio of 0.47 (almost similar to that of the small-size fiber). From now on, they will be named 66 ϕ LC-mPOF and 100 ϕ LC-mPOF, respectively.

C. Experimental Methods

1) mPOF end-Face Modification for Selective Filling: In order to obtain a LC-mPOF, the hollow-core of the fiber has to be filled selectively. This was achieved by a slight modification on the lower end-face of the probe: the holes of the cladding were sealed and the hollow-core was left open. This was done following the two-step procedure described in literature [23], [24]. Briefly, NOA 65 was solved in isopropyl alcohol 1/4 v/v. Afterwards, the end-face (Fig. 4a) of the probe was immersed for 5 s in the solution and the adhesive was cured with an UV lamp. Since the filling speed of the capillary effect is closely related to the diameter of the hole, the adhesive reached more height in the hollow-core than in the holes of the cladding; this way,

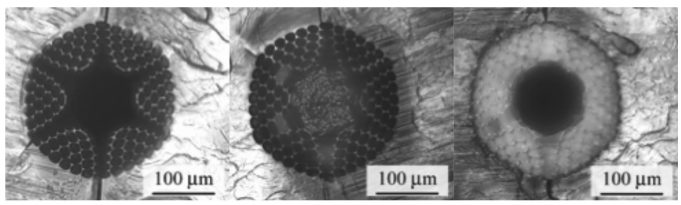

a) Unmodified end-face. b) Sealed core but open cladding intermediate step. c) Sealed cladding end-face.

Fig. 4. Microscope images in different steps for the modification of the end-face of the probe.

the fiber was cleaved between these two distances, leading to a sealed core but an open cladding end-face (Fig. 4b). Then, this end-face was immersed again in the solution for 10 s and cured. The adhesive filled only the holes of the cladding and it reached higher than the adhesive previously cured in the hollow-core. Finally, the fiber was cleaved in between and the sealed cladding end-face was obtained (Fig. 4c).

2) Measurement Set-Up: Two different set-ups were configured. The first one was employed to measure the Raman spectra of the solution in the cuvette: a simple polycarbonate cuvette was filled with the solution containing the target sample and the upper surface was focused with the microscope. The second set-up was used to measure the Raman spectra in the sensing platform with LC-mPOFs: the unmodified end-face of the probe was held upwards using a holder, and the opposite and modified end-face was immersed in the solution, as can be seen in Fig. 5. The same set-up was used either for the 66 ϕ LC-mPOF or for the

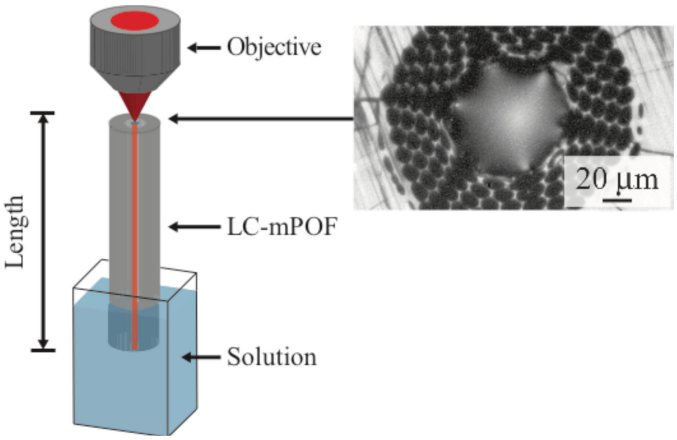

Fig. 5. Experimental set-up and the immersion of the modified end-face of the LC-mPOF. The inset shows the upper end-face focused by the Raman microscope.

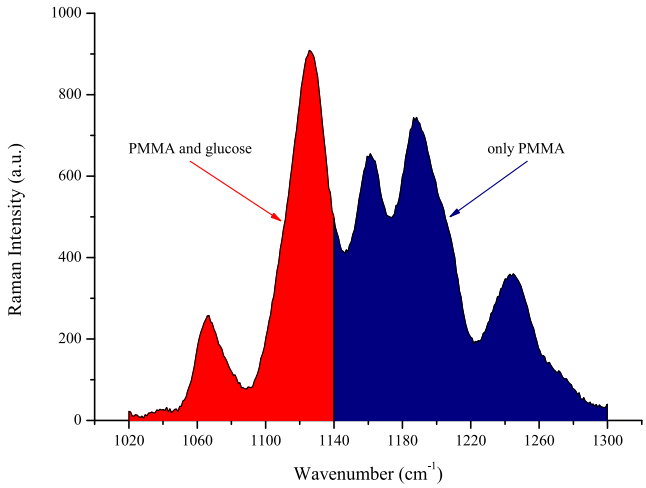

Fig. 6. Raman spectrum of the LC-mPOF filled with a glucose solution; representation of the areas used for the glucose quantification, the area contributed by PMMA and glucose in red, and the area of only PMMA in blue.

100 ϕ LC-mPOF. The central hollow-core of each probe was filled with the solution containing the target sample by capillary effect in a short period of time (≈30 s.). For instance, and using 10-cm-long fibers, only 1.33 μl of solution were necessary in the 66 ϕ LC-mPOF and 3.14 μl in the 100 ϕ LC-mPOF. Once the LC-mPOF was completely filled, the launching laser beam was focused in the center of the core and, finally, the Raman spectrum was measured.

All the measured spectra were recorded using a Renishaw (Gloucestershire, UK) inVia confocal Raman Microscope. A near infrared 785-nm-wavelength laser was used as the excitation source and only 10% of the maximum power was launched on the sample (more specifically, 27.61 mW). The acquisition time for each experiment was set to 10 s in order to avoid any thermal effect either in the solution or in the structure of the LC-mPOF. The spectra were recorded from 100 cm^{-1} to 3200 cm^{-1}. Both set-ups employed a 50 X objective with a 0.75 NA from Leica (Wetzlar, Germany).

D. Data-Processing

Considering that the overprocessing of the measured spectra could hide crucial information about the concentration of the target sample, extreme care was taken for data processing. For that reason, only the baselines of the spectra were subtracted using the *Fill Peaks* algorithm from the *Baseline* package of R software [25], and any further processing was discarded. Additionally, the spectra were managed with a package called *hyperSpec* [26].

Regarding the SNR determination, potassium ferricyanide ($K_3[Fe(CN)_6]$) was added to the solutions containing the target sample and its unique peak, placed at 2140 cm^{-1}, was taken as a reference signal (see the Appendix for further details about its spectra). Since this peak is separated from the spectral region of the Raman peaks of the PMMA and the target sample, there were no interferences [27]. This peak was Gaussian fitted and the SNR was calculated following (1):

$$\mathrm{SNR} = \frac{\text{Intensity at } 2140\ \mathrm{cm}^{-1}}{\sigma^2\ (\text{non-signal region})}, \tag{1}$$

where σ is the standard deviation of a range in the spectra without peaks, i.e., its mean value is equal to zero.

Prior to quantifying the concentration of glucose, the following issue had to be addressed: since the main peak of the glucose is placed at 1127 cm^{-1} [6], it interfered with a strong peak from the vibrations ν(C–O) and ν(C–COO) belonging to PMMA, because the latter appears at the same wavenumber, i.e., at 1127 cm^{-1} [20]. Nevertheless, the Raman signal of glucose could unambiguously be identified (see the Appendix for further details). The chosen approach for quantification was to calculate a ratio of areas between specific ranges in the spectra, from now on denoted by area-ratio, as shown in (2) and Fig. 6:

$$\text{Area-ratio} = \frac{\text{Area from } 1020\ \mathrm{cm}^{-1} \text{ to } 1140\ \mathrm{cm}^{-1}}{\text{Area from } 1140\ \mathrm{cm}^{-1} \text{ to } 1300\ \mathrm{cm}^{-1}} \tag{2}$$

This way, measurements obtained from a solution without glucose resulted in a low area-ratio. However, the area-ratio increases with the glucose concentration as the area from 1020 cm^{-1} to 1140 cm^{-1} is larger due to the contribution of glucose.

III. Results and Discussion

In order to analyze the suitability of the LC-mPOF probes for therapeutic glucose monitoring during SGLT2 inhibitor therapy, the system was subjected to various tests involving the quantification of glucose in low concentration solutions. The first step was to find the best Raman signal enhancement provided by each LC-mPOF fiber and to determine the most suitable diameter of the LC-mPOF and the optimum length of the fiber probe. For this purpose, the unique peak of $K_3[Fe(CN)_6]$ at 2140 cm^{-1} was monitored.

A. SNR Enhancement for $K_3[Fe(CN)_6]$ and Selection of the Optimum Length of the Fiber Probe

Solutions were prepared with six different concentrations of glucose, ranging from 0 mmol/L to 25 mmol/L in steps of 5 mmol/L; all solutions contained 25 mmol/L of $K_3[Fe(CN)_6]$.

TABLE I
SNR OF THE DIFFERENT SET-UPS

Set-up	SNR
Cuvette	32 ± 1
66 ϕ LC-mPOF	1220 ± 40
100 ϕ LC-mPOF	680 ± 20

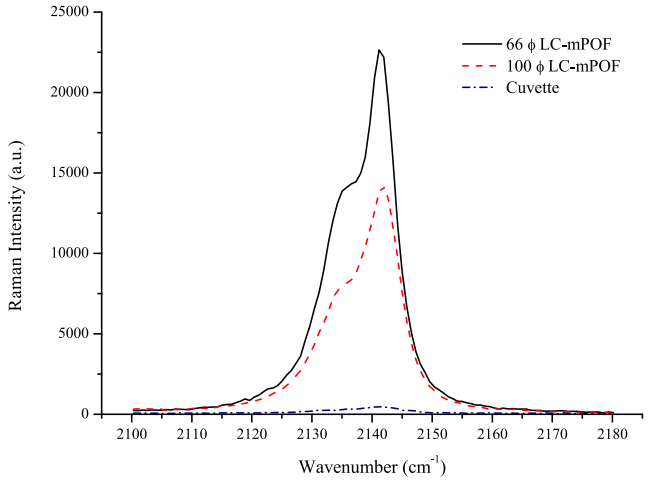

Fig. 7. Comparison of the Raman average spectra of $K_3[Fe(CN)_6]$ around 2140 cm^{-1} for the cuvette and both fiber sizes.

The objective was three-fold: to quantify the enhancement provided by the use of different diameter LC-mPOFs, and to check whether that enhancement depended on the glucose concentration and/or on the length of the probe.

For both LC-mPOF fiber sizes, the precise focusing of the launching beam on the fiber-core was critical if FERS measurements were to be valid. Therefore, threshold values of SNR were defined. Regarding the 66 ϕ LC-mPOF, acquisitions with SNR values below 1000 were discarded. As for the 100 ϕ LC-mPOF, acquisitions with SNR values below 500 were discarded. Discards were made under the assumption that, in those cases, the incident spot was not properly focused on the core.

Table I shows the SNR values obtained from all valid measurements for the cuvette and for both fiber sizes regarding the Raman peak of $K_3[Fe(CN)_6]$ at 2140 cm^{-1}.

From the SNR values, it can be observed that the best Raman signal enhancement is achieved with the 66 ϕ LC-mPOF probe. Besides, it can be concluded that, in comparison with the cuvette, using the same configuration, the enhancement of the SNR values reaches up to 37 times for the 66 ϕ LC-mPOF and 21 times for the 100 ϕ LC-mPOF in comparison with the cuvette. This behavior can be seen in the average intensities of the peak located in 2140 cm^{-1} for the different set-ups, shown in Fig. 7 (as for the extended spectra, please refer to Fig. 16).

Secondly, the performed SNR measurements of the LC-mPOFs were split, taking into account the glucose concentration. Detailed results can be seen in Fig. 8 (the vertical bars denote the uncertainty associated with each measurement).

From this chart, it can be concluded that the different glucose concentrations do not affect the intensity of the unique peak of $K_3[Fe(CN)_6]$, neither the SNR values as expected. The

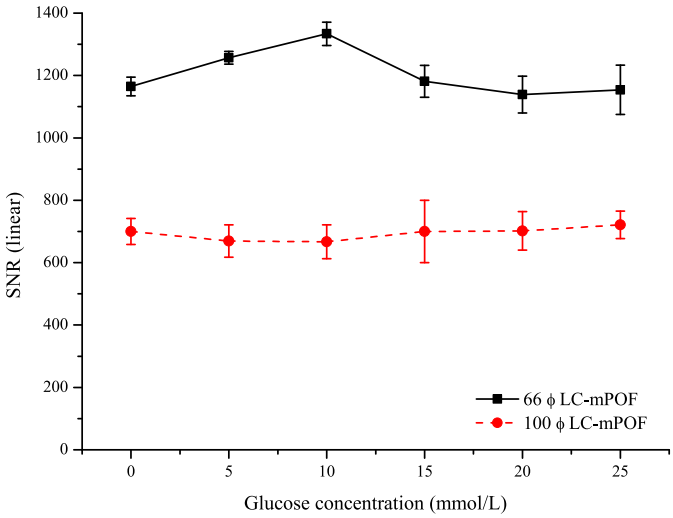

Fig. 8. SNR values of the 2140 cm^{-1} centered peak belonging to $K_3[Fe(CN)_6]$ and according to several glucose concentrations.

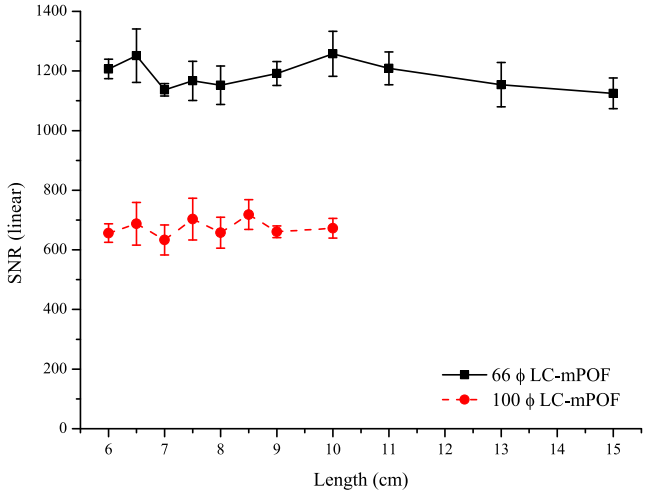

Fig. 9. SNR values of the 2140 cm^{-1} centered peak belonging to $K_3[Fe(CN)_6]$ and according to several probe lengths.

standard deviation of the SNR values measured for the solutions of different glucose concentration is lower than 10% for both fiber diameters (notice that the $K_3[Fe(CN)_6]$ concentration, 25 mmol/L, is always the same in all these measurements). The slight variations observed in Fig. 8 may be attributed to focusing divergences and/or to slight variations on the concentration due to preparation uncertainties.

Lastly, different fiber lengths were measured. At this point, it is noteworthy to mention that, for the 100 ϕ LC-mPOF, it was not possible to fill the core by capillary effect for lengths exceeding 10 cm, because the central core diameter was too big to allow proper filling by capillary effect. For the 66 ϕ LC-mPOF, lengths from 6 cm up to 15 cm were measured instead. Obtained results are displayed in Fig. 9.

It can be seen that the SNR does not improve with the length, because fiber losses compensate the enhancement in the Raman spectra intensity at longer interaction lengths. The standard deviation in this range is of 3.88% for the 66 ϕ LC-mPOF and of 4.53% for the 100 ϕ LC-mPOF. In accordance with the results,

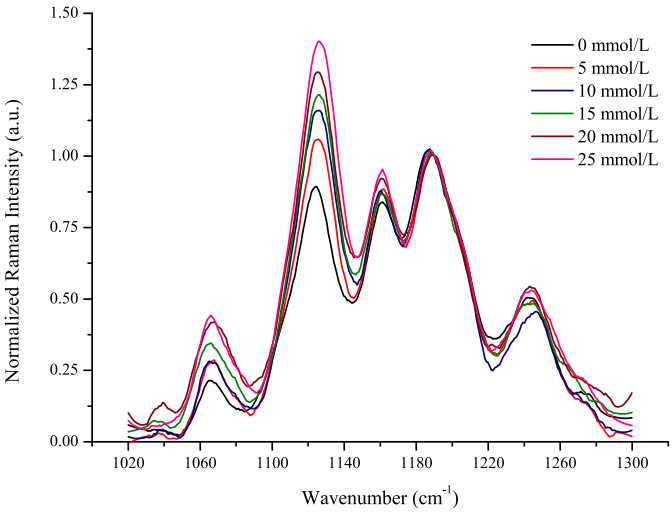

Fig. 10. Raman spectra normalized for the peak at 1190 cm^{-1} for different glucose concentrations measured in 10-cm-long 66 ϕ LC-mPOF.

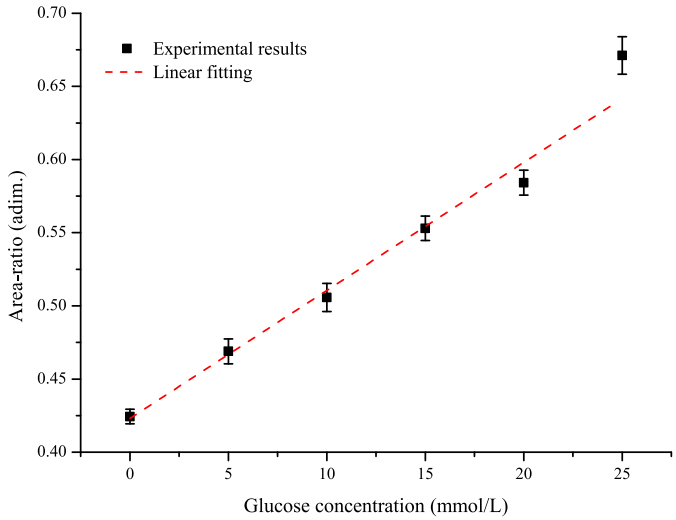

Fig. 11. Experimental area-ratio measurements and linear calibration curve for the analyzed glucose concentrations for the 66 ϕ LC-mPOF.

the glucose concentration measurements shown in the forthcoming section were performed using 10-cm-long fiber probes, since such a length provided easy-to-handle probes and, at the same time, reasonably low volume quantities were required.

B. Glucose Quantification

With the aim of testing the suitability of the LC-mPOF-based FERS sensing platform as a glucose sensor in a clinically relevant range, measurements were performed with 10-cm-long 66 ϕ and 100 ϕ LC-mPOFs, and the spectra were processed as explained in Section II-D.

Again, 0, 5, 10, 15, 20, and 25 mmol/L glucose solutions were quantified (together with 25 mmol/L of $K_3[Fe(CN)_6]$). These quantities were chosen on the basis of the following facts: during the SGLT2 inhibitor therapy, daily glucose losses are usually between 70–120 g [28], and urinary glucose concentrations vary from 5 mmol/L (100 mg/dl) to 17 mmol/L (300 mg/dl) approximately after 6 hours of SGLT2-inhibitor ingestion [29].

For each of the six glucose concentrations, at least three high SNR measurements were performed with each of the fiber sizes, and the area-ratio was calculated using (2). From the average measured spectra, there is an increase in the intensity of the Raman peaks at 1127 cm^{-1} and 1066 cm^{-1}, which correspond to glucose, whereas the Raman peak of PMMA at 1190 cm^{-1} is constant. The ratio of these regions is charted in Fig. 10. It is also remarkable that such glucose concentrations could not be measured using the cuvette set-up.

From these spectra, it can be observed that even slight variations of 5 mmol/L of the glucose concentration are detected. Figures 11 and 12 show the area-ratio for experimental results and the linear fitting for the 66 ϕ LC-mPOF and for the 100 ϕ LC-mPOF, respectively.

From the experimental results, it can be proved that a minimum sensitivity threshold of 5 mmol/L is achieved in the FERS sensing platform for the 66 ϕ LC-mPOF. For the 100 ϕ LC-mPOF, whose higher standard deviations for different measurements make this fiber less suitable, it cannot be ensured the

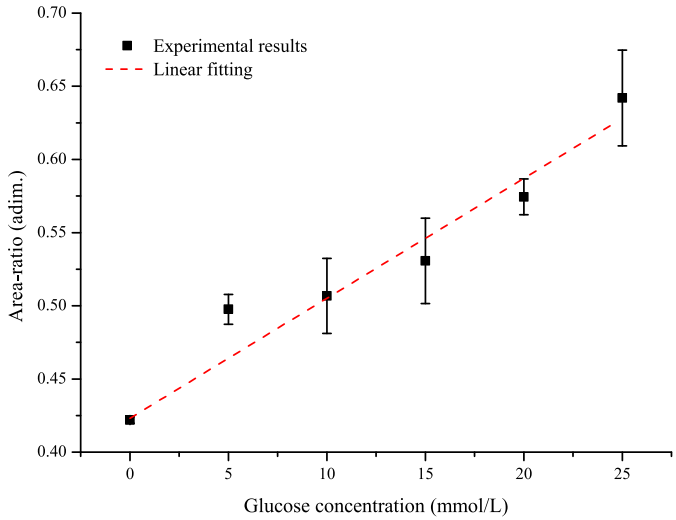

Fig. 12. Experimental area-ratio measurements and linear calibration curve for the analyzed glucose concentrations for the 100 ϕ LC-mPOF.

sensitivity provided by the smaller size LC-mPOF. The values of the Pearson correlation coefficient (r) for the linear fitting are 0.992 for the 66 ϕ LC-mPOF and 0.975 for the 100 ϕ LC-mPOF, respectively.

Furthermore, the Limit Of Detection (LOD) and the Limit Of Quantification (LOQ) are calculated according to the well-known formulas given by (3) and (4) [30]:

$$\mathrm{LOD} = 3\sigma^2/S, \tag{3}$$

$$\mathrm{LOQ} = 10\sigma^2/S, \tag{4}$$

where σ is the standard deviation of the linear fitting and S the slope. For the 66 ϕ LC-mPOF, the LOD is 0.183 mmol/L and the LOQ is 0.612 mmol/L. For the case of the 100 ϕ LC-mPOF, the LOD is 0.338 mmol/L and the LOQ is 1.129 mmol/L. These results demonstrate the feasibility of this novel and easily affordable LC-mPOF-based FERS sensing platform to monitor

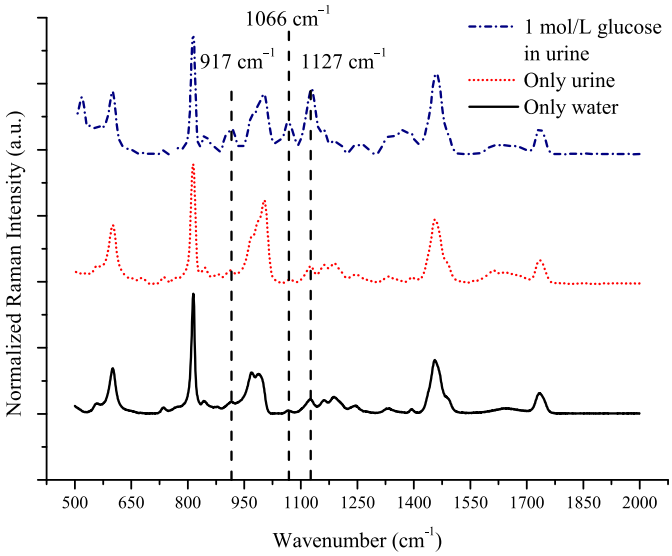

Fig. 13. Raman spectra of water (black), urine (red), and 1 mol/L glucose in urine (blue) in the 66 ϕLC-mPOF.

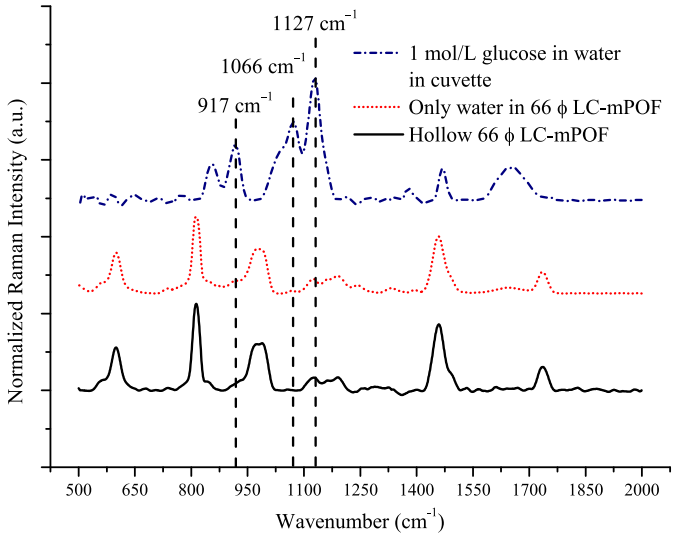

Fig. 14. Raman spectra of 1 mol/L of glucose in water (blue line), and the 66 ϕ LC-mPOF either filled with water (red line) or hollow (black line).

glucose in aqueous media in the clinically relevant concentration range.

C. First Measurements in Urine

Additionally, preliminary tests were carried out to detect glucose in real human urine using the sensing platform with the 66 ϕ LC-mPOF. Previously, it was checked that the Raman spectrum of the urine used in the experiments was in agreement with other reported results [31]: according to the measurements, the most prominent Raman peak of urine arises around 1000 cm^{-1} and, therefore, it does not interfere with the other Raman peaks of interest. Figure 13 displays the spectrum of the glucose in urine (1 mol/L) in comparison with the spectra of the fibers filled only with urine or water, respectively. The main Raman peaks of glucose are also highlighted there.

All in all, this proof-of-principle study proved that the presented sensing platform has great potential for further studies in biological fluids such as urine, paving the way for a potential monitoring device in SGLT2 inhibitor therapy. In other words, this study provides evidence that the proposed method is promising for clinical use, which is a prerequisite for further studies in order to validate the method.

IV. Conclusions

A new LC-mPOF based FERS sensing platform has been designed and implemented for low concentration glucose detection in aqueous solution. The LC-mPOF probes have been specially designed and fabricated for this aim, and two different diameters of the same LC-mPOF geometry have been employed in order to find out the design of better performance. The set-up using LC-mPOFs provides a Raman signal enhancement above one order of magnitude in comparison to conventional cuvette measurements. These results enable the detection and quantification of low glucose concentrations, with a LOQ value of 0.621 mmol/L and a LOD value of 0.186 mmol/L for the LC-mPOF with a 66-μm-diameter core. Thus, this platform is suitable for the detection of clinically relevant glucose concentrations, showing a great potential for urinary glucose monitoring in a SGLT2 inhibitor therapy. The volume of solution used in the measurements is of 1.33 μl for the LC-mPOF with a 66-μm-diameter core and a length of 10 cm, and, therefore, this sensing platform might be an ideal candidate for accurate and low-cost biosensing applications. Preliminary measurements in urine have also been carried out and the feasibility of the platform has been demonstrated.

Appendix

The prominent Raman peaks of glucose, placed at 917, 1066 and 1127 cm^{-1}, are overlapped by several strong peaks of PMMA, as it can be seen in Fig. 14.

However, it is possible to obtain the differentiated spectrum of glucose by removing the background spectrum of water. This is achieved by subtracting the spectrum of water in 66 ϕ LC-mPOF (refer back to Fig. 14) from the spectrum measured for a certain concentration of glucose in 66 ϕ LC-mPOF. For instance, Fig. 15 shows the differentiated spectrum of 25 mmol/L of glucose.

The differentiated spectrum shows clearly the prominent Raman peaks of glucose. The presence of these peaks leads to an increase in the area-ratio used for glucose quantification.

Finally, Fig. 16 shows the extended Raman spectra of a solution containing 25 mmol/L of $K_3[Fe(CN)_6]$. The Raman peak used as a reference signal is placed at 2140 cm^{-1}. Even though the Raman spectrum in the cuvette is much cleaner (compare the Raman peaks of PMMA in the 66 ϕ LC-mPOF for lower wavenumbers), the Raman peak at 2140 cm^{-1} is much weaker. In contrast, this Raman peak stands out clearly in the 66 ϕ LC-mPOF and it is separated from the spectral region of other Raman peaks of PMMA. As a consequence, the reference signal of $K_3[Fe(CN)_6]$ can be measured in the 66 ϕ LC-mPOF without any interference.

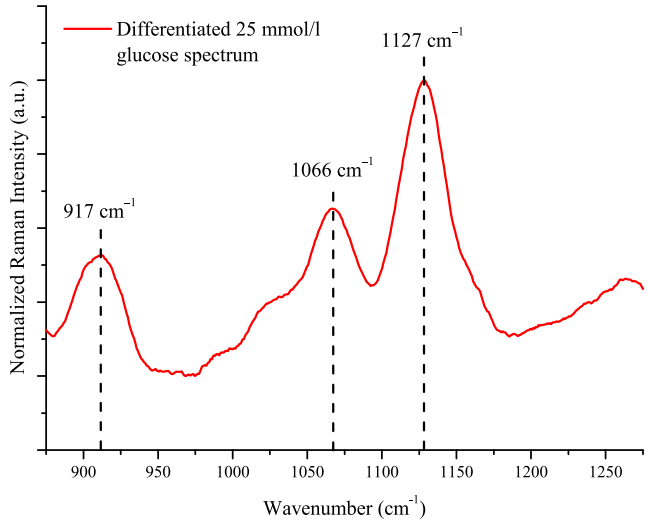

Fig. 15. Differentiated Raman spectrum of 25 mmol/L glucose in the 66 ϕ LC mPOF from the spectrum of water measured in the 66 ϕ LC mPOF.

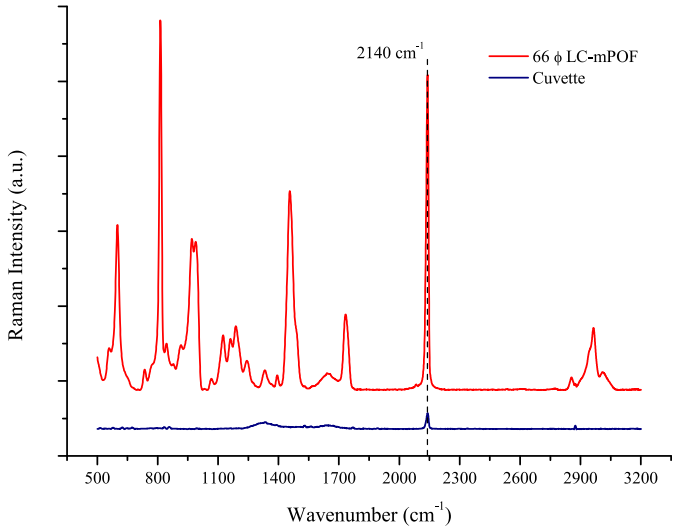

Fig. 16. Extended Raman spectra urine measured in the 66 ϕ LC mPOF and in the cuvette.

ACKNOWLEDGMENT

The authors are also grateful to the technical and human support provided by SGIKER (UPV/EHU, MICINN, GV/EJ, ERDF, and ESF).

REFERENCES

[1] WHO, *Diabetes Mellitus, Fact Sheet N°138*. Geneva, Switzerland: WHO Media Centre, 2018.
[2] F. Gomez-Peralta *et al.*, "Practical approach to initiating SGLT2 inhibitors in type 2 diabetes," *Diabetes Therapy*, vol. 8, no. 5, pp. 953–962, 2017.
[3] S. Riser Taylor and K. B. Harris, "The clinical efficacy and safety of sodium glucose cotransporter-2 inhibitors in adults with type 2 diabetes mellitus," *Pharmacotherapy*, vol. 33, no. 9, pp. 984–999, 2013.
[4] *FDA Warns About Rare Occurrences of a Serious Infection of the Genital Area With SGLT2 Inhibitors for Diabetes*, US FDA, Silver Spring, MD, USA, Saf. Announc., Drug Safety, 2018.
[5] S. R. Kim *et al.*, "Morning spot urine glucose-to-creatinine ratios predict overnight urinary glucose excretion in patients with type 2 diabetes," *Ann. Lab. Med.*, vol. 37, no. 1, pp. 9–17, 2017.
[6] J. Shao *et al.*, "In vivo blood glucose quantification using Raman spectroscopy," *PLoS One*, vol. 7, no. 10, Oct. 2012, Paper no. e48127.
[7] J. L. Lambert, C. C. Pelletier, and M. Borchert, "Glucose determination in human aqueous humor with Raman spectroscopy," *J. Biomed. Opt.*, vol. 10, no. 3, 2005, Paper no. 031110.
[8] O. Lyandres *et al.*, "Progress toward an in vivo surface-enhanced Raman spectroscopy glucose sensor," *Diabetes Technol. Therapeutics*, vol. 10, no. 4, pp. 257–265, Aug. 2008.
[9] T. Frosch, D. Yan, and J. Popp, "Ultrasensitive fiber enhanced UV resonance raman sensing of drugs," *Anal. Chem.*, vol. 85, no. 13, pp. 6264–6271, Jul. 2013.
[10] D. Yan *et al.*, "Fiber enhanced Raman spectroscopic analysis as a novel method for diagnosis and monitoring of diseases related to hyperbilirubinemia and hyperbiliverdinemia," *Analyst*, vol. 141, no. 21, pp. 6104–6115, 2016.
[11] D. Yan, J. Popp, M. W. Pletz, and T. Frosch, "Fiber enhanced Raman sensing of levofloxacin by PCF bandgap-shifting into the visible range," *Anal. Methods*, vol. 10, no. 6, pp. 586–592, 2018.
[12] D. Yan, J. Popp, M. W. Pletz, and T. Frosch, "Highly sensitive broadband Raman sensing of antibiotics in step-index hollow-core photonic crystal fibers," *ACS Photon.*, vol. 4, no. 1, pp. 138–145, 2017.
[13] D. Yan *et al.*, "Fiber-enhanced Raman sensing of cefuroxime in urine," *Anal. Chem.*, vol. 90, pp. 13243–13248, 2018.
[14] A. Knebl, D. Yan, J. Popp, and T. Frosch, "Fiber enhanced raman gas spectroscopy," *Trends Anal. Chem.*, vol. 103, pp. 230–238, 2018.
[15] X. Yang *et al.*, "Hollow-core photonic crystal fibers for surface-enhanced raman scattering probes," *Int. J. Opt.*, vol. 2011, 2011, Paper no. 754610.
[16] A. Khetani *et al.*, "Hollow core photonic crystal fiber as a reusable Raman biosensor," *Opt. Express*, vol. 21, no. 10, pp. 12340–12350, 2013.
[17] U. S. Dinish *et al.*, "Highly sensitive SERS detection of cancer proteins in low sample volume using hollow core photonic crystal fiber," *Biosens. Bioelectron.*, vol. 33, no. 1, pp. 293–298, Mar. 2012.
[18] J. C. Knight, "Photonic crystal fibres," *Nature*, vol. 424, no. 6950, pp. 847–851, Aug. 2003.
[19] M. Azkune *et al.*, "U-shaped and surface functionalized polymer optical fiber probe for glucose detection," *Sensors*, vol. 18, no. 1, 2018, Paper no. 34.
[20] K. J. Thomas *et al.*, "Raman spectra of polymethyl methacrylate optical fibres excited by a 532 nm diode pumped solid state laser," *J. Opt. A, Pure Appl. Opt.*, vol. 10, no. 5, May 2008, Paper no. 055303.
[21] H. Willis, V. J. Zichy, and P. Hendra, "The laser-raman and infra-red spectra of poly(methyl methacrylate)," *Polymer*, vol. 10, pp. 737–746, Jan. 1969.
[22] E. Arrospide *et al.*, "Polymers beyond standard optical fibres—Fabrication of microstructured polymer optical fibres," *Polym. Int.*, vol. 67, no. 9, pp. 1155–1163, Sep. 2018.
[23] Y. Huang, Y. Xu, and A. Yariv, "Fabrication of functional microstructured optical fibers through a selective-filling technique," *Appl. Phys. Lett.*, vol. 85, no. 22, pp. 5182–5184, Nov. 2004.
[24] K. Nielsen *et al.*, "Selective filling of photonic crystal fibres," *J. Opt. A, Pure Appl. Opt.*, vol. 7, no. 8, pp. L13–L20, 2005.
[25] K. H. Liland, "Baseline: Baseline correction of spectra," *R Package* Version 2.15, Jul. 5, 2015. [Online]. Available: https://CRAN.R-project.org/package=baseline
[26] C. Beleites and V. Sergo, "HyperSpec: A package to handle hyperspectral data sets in R," R Package Version 2.15, Jun. 28, 2018. [Online]. Available: https://CRAN.R-project.org/package=hyperSpec
[27] Z. Iqbal, "Raman scattering and the electronically-induced phase transition in $K_3Fe(CN)_6$ at 130 K," *J. Phys. C, Solid State Phys.*, vol. 10, no. 18, pp. 3533–3543, Sep. 1977.
[28] S. Chaplin, "SGLT2 inhibitors and risk of genitourinary infections," *Prescriber*, vol. 27, no. 12, pp. 26–30, 2016.
[29] A. Tahara *et al.*, "Characterization and comparison of sodium-glucose cotransporter 2 inhibitors in pharmacokinetics, pharmacodynamics, and pharmacologic effects," *J. Pharmacol. Sci.*, vol. 130, no. 3, pp. 159–169, 2016.
[30] A. Shrivastava and V. Gupta, "Methods for the determination of limit of detection and limit of quantitation of the analytical methods," *Chronicles Young Sci.*, vol. 2, no. 1, pp. 21–25, 2011.
[31] W. R. Premasiri, W. Ranjith, R. H. Clarke, and M. E. Womble, "Urine analysis by laser Raman spectroscopy," *Lasers Surg. Med.*, vol. 28, no. 4, pp. 330–334, 2011.